

Supporting Information

Overcoming the Phase Separation within High-Entropy Metal Carbide by Poly(ionic liquid)s

Yan Leng^{a,b}, Zihao Zhang^b, Hao Chen^b, Shengyu Du^{a,c}, Jixing Liu^b, Shiyang Nie^c, Yuming Dong^a,
Pengfei Zhang^{c,*}, Sheng Dai^{b,d,*}

^[a] The Key Laboratory of Synthetic and Biological Colloids, Ministry of Education. School of Chemical and Material Engineering, Jiangnan University, Wuxi 214122, Jiangsu, China.

^[b] Department of Chemistry, University of Tennessee, Knoxville, TN 37996, USA.

^[c] School of Chemistry and Chemical Engineering. Shanghai Jiao Tong University, Shanghai 200240, P. R. China.

^[d] Chemical Sciences Division, Oak Ridge National Laboratory Knoxville, TN 37831, USA.

Characterization

The materials' structure and chemistry were characterized using a Hitachi HF-3300 field-emission transmission electron microscope operating at 200 kV for imaging (SEM and ADF STEM) and EDS elemental mapping (Bruker silicon drift EDS detector). HRTEM images were acquired using an aberration-corrected FEI Titan system operating at 200 kV. A OneView Camera was used to capture the HRTEM images with a 4 K × 4 K resolution. X-ray photoelectron spectroscopy (XPS) measurement was conducted with a Thermo Fisher K-Alpha (USA) with an Al K α radiation as the X-ray source. The crystal phase of the material was measured on a PANalytical diffractometer using Cu K α radiation. The thermal decomposition behavior of the material was monitored at a heating rate of 10°C min⁻¹ in air with a flow rate of 40 mL min⁻¹ using a TGA unit. N₂ adsorption-desorption isotherm was performed at 77 K using a TriStar (Micromeritics Instrument Corp.; Norcross, GA, USA) analyzer. Raman analysis was performed using a Perkin Elmer-Raman Station 400F spectrometer equipped with a liquid N₂ cooled charge-coupled device detector and a

confocal microscope. A 350 mW near-infrared 785 nm laser was used for analysis under ambient conditions. XRD patterns were collected on the Bruker D8 Advance powder diffractometer using Ni-filtered Cu/K α radiation source at 40 kV and 20 mA, from 5° to 90° with a scan rate of 2°/min. The high-angle annular dark-field scanning TEM (HAADF-STEM) images were performed on a Talos F200X instrument.

Experimental Section

Synthesis of 3-cyano-1-vinylimidazolium bromide ([CIM]Br):

1-vinylimidazole (0.1 mol, 9.4 g), bromoacetonitrile (0.1 mol, 11.9 g), and acetone (50 mL) were added into a 100 mL round-bottom flask. The mixture was heated to 60 °C with stirring for 24 h. On completion, the produced white solid powder was filtered and washed with acetone for three times, and then dried at 50 °C in vacuum to give [CIM]Br.

Synthesis of poly(3-cyano-1-vinylimidazolium bromide) ([PCIM]Br), poly(3-butyl-1-vinylimidazolium bromide) ([PBIM]Br), poly(1-cyano-4-vinylpyridine bromide) ([PCPy]Br), [PCIM]Br, and [PCIM]DCD:

Polymer(vinylimidazole) was first prepared *via* the polymerization of 1-vinylimidazole (0.1 mol, 9.4 g) using azodiisobutyronitrile (AIBN, 0.2 g) as initiator in acetone (50 mL). The mixture was stirred at 60 °C for 24 h, and white solid powder was formed. After that, bromoacetonitrile (0.1 mol, 11.9 g) was added into the mixture and continue to react for 24 h. After cooling to room temperature, the precipitate was separated by centrifugation, washed with ethanol for three times, and dried at 80 °C overnight to afford the [PCIM]Br. Based on the similar procedure, [PCPy]Br can be obtained when 1-vinylimidazole was changed to vinylpyridine, and [PBIM]Br can be obtained when bromine acetonitrile was changed to 1-bromobutane.

The obtained [PCIM]Br (2 g) was dissolved in 20 mL of deionized water, and NaBF₄ (1 g) was dissolved in 10 mL of deionized water. The NaBF₄ solution was added slowly in to the [PCIM]Br solution under ice bath condition, forming light yellow solid. The mixture was stirred for another 12 h at room temperature. On completion, the solid product was centrifuged, washed, and dried at 60 °C to yield [PCIM]BF₄. Based on the similar procedure, using sodium dicyandiamide (0.83 g) instead of NaBF₄, [PCIM]DCD can be obtained.

Synthesis of HMC@NC-t (t stands for pyrolysis temperature)

In a typical synthesis, equimolar (0.5 mmol) MoCl₅ (Alfa Aesar, 99.6%), WCl₅ (Alfa Aesar, 99.6%), VCl₃ (Sigma-Aldrich, 97%), CrCl₃ (Acros, 99%), and NbCl₅ (Acros, 99.8%), were mixed with 1.2 g [PCIM]Br. The composite was added into a 35 mL zirconia vial reactor along with three zirconia balls. The reactor was placed in a high-speed vibrating ball miller (1200 rounds min⁻¹, 300 W motor power) and the mixtures were ball milled for 1 h. The mixed solid powder (denoted as [PCIM]Br-MCl_x) was pyrolyzed at 900°C for 3 h with heating rate of 5°C min⁻¹ under an N₂ atmosphere. The obtained black sample was denoted as HMC@NC-900. Other control samples were prepared based on the same method by introducing TiCl₄, HfCl₄, ZrCl₄, TaCl₅, or NH₄VO₃ as metal sources.

Ethylbenzene dehydrogenation with CO₂

The catalyst was evaluated for CO₂-DEB in a fixed bed reactor from 350 to 550°C under atmospheric pressure. Firstly, 0.2g of the catalyst (40–60 mesh) diluted with the same amount of quartz sands (40–60 mesh) was loaded into the reactor. After pretreating with CO₂ at target temperature for 15min., the analytical grade EB was introduced into the reactor by an HPLC pump at 0.02 mL·min⁻¹, and the molar ratio of CO₂/EB=5 was kept the same for all of the tests. The liquid products including benzene, toluene, styrene, and unreacted EB were in situ analyzed on a gas chromatograph with an HP-5 capillary column (0.25 mm×30m) and a FID detector.

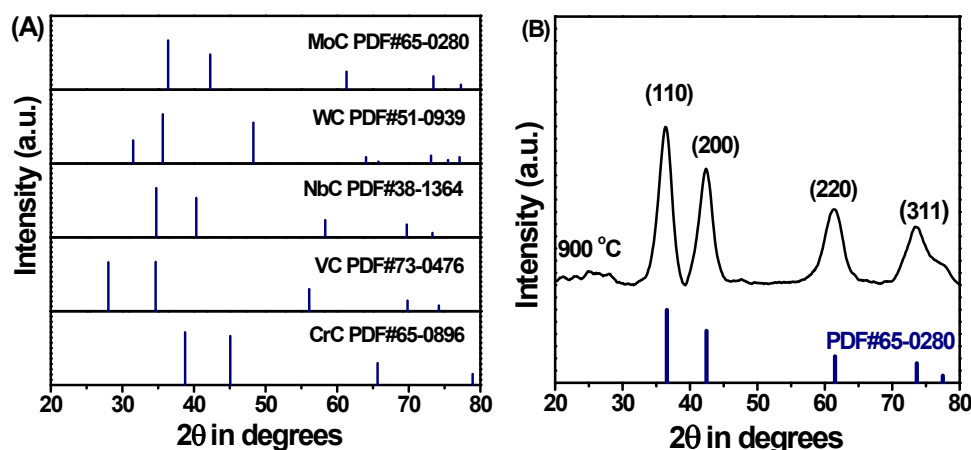


Figure S1.(A) Standard XRD patterns of five metal carbides (MoC, WC, NbC, VC, CrC); (B) XRD pattern of HMC@NC-900.

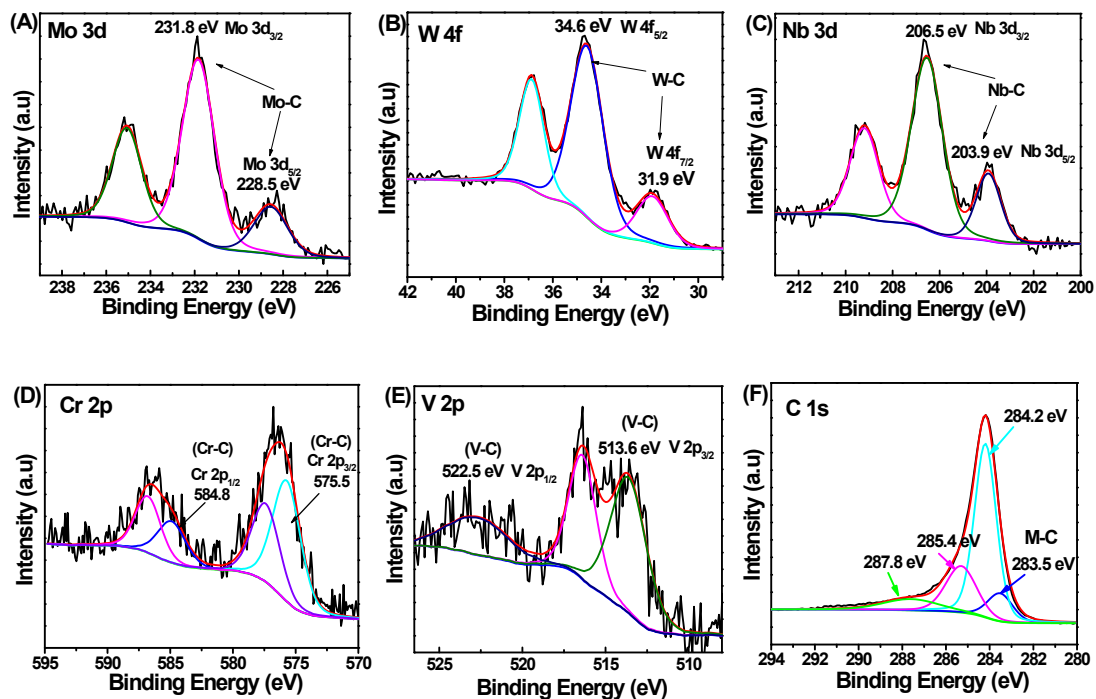


Figure S2. High-resolution XPS spectra of Mo 3d (A), W 4f (B), Nb 3d (C), Cr 2p (D), V 2p (E) C 1s (F) for HMC@NC-900.

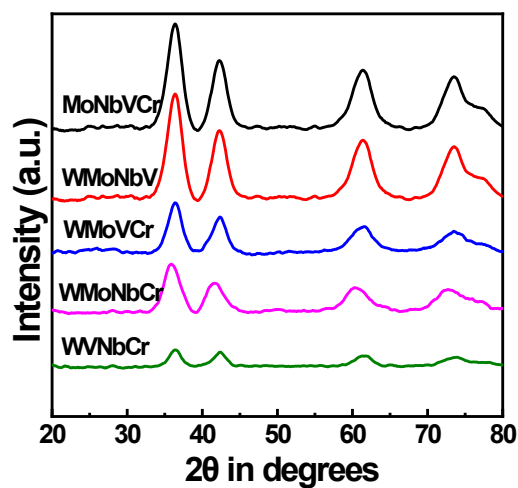


Figure S3. XRD patterns for four-metallic carbides derived from MCl_x and $[PCIM]Br$

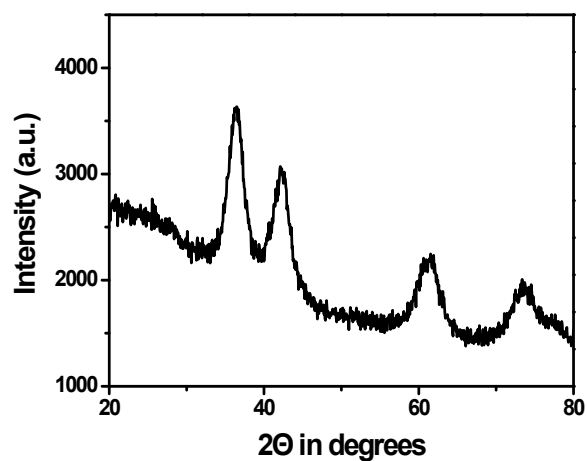


Figure S4. XRD pattern of HMC@NC-900 using NH_4VO_3 instead of VCl_3 as metal precursor.

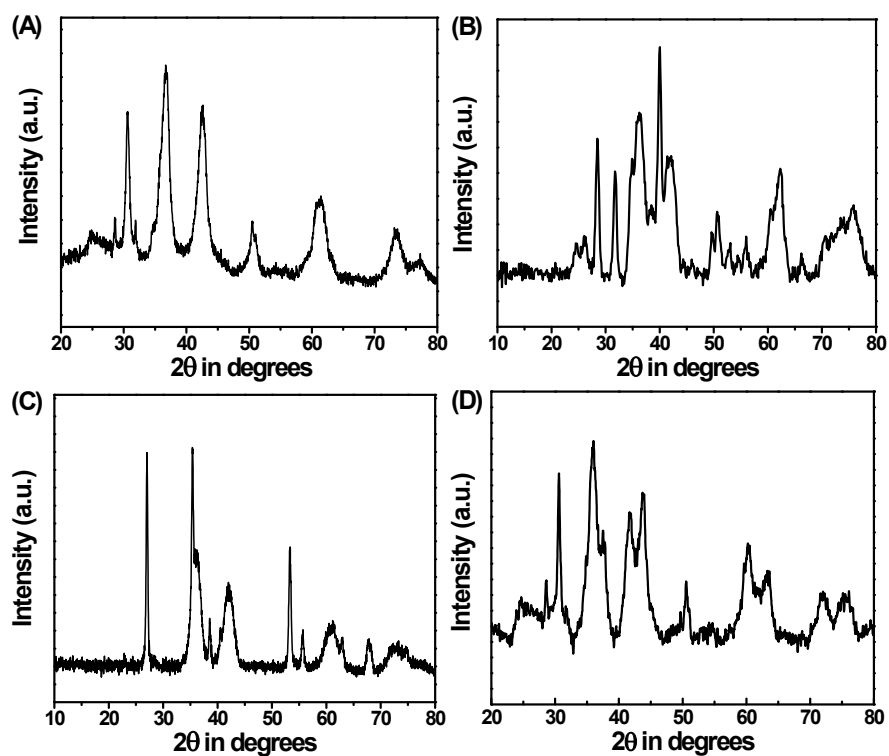


Figure S5. XRD patterns of metallic carbides containing (A) WMoNbVZr, (B) WMoNbVHf, (C) WMoNbVTa, (D) WMoNbVTi.

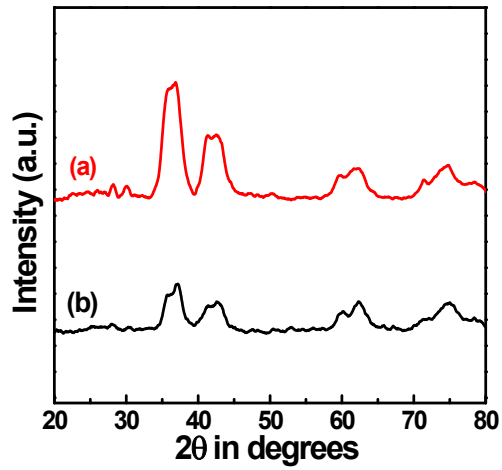


Figure S6. XRD patterns for HMC@NC-900 derived from five MCl_x ($M = Mo, W, V, Cr, Nb, x = 3-5$) and different organic carbon sources (a) poly(vinyl pyrrolidone) (PVP) and (b) poly(vinylimidazole) (PVIM).

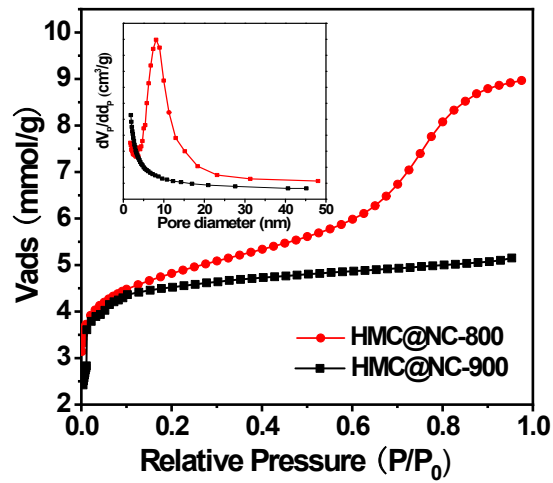


Figure S7. N_2 adsorption isotherms and pore size distributions of HMC@NC-800 and HMC@NC-900.

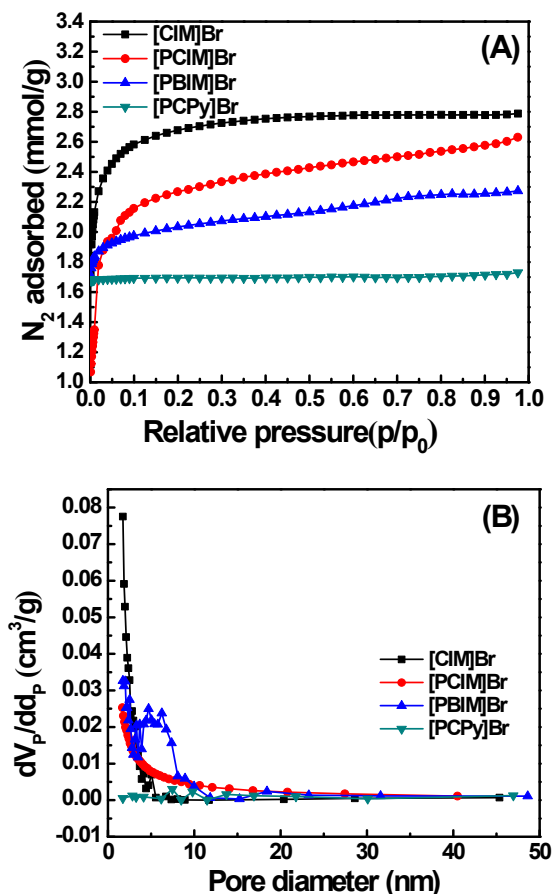


Figure S8. N_2 adsorption isotherms (77 K) and BJH pore-size distributions for HMC@NC-900 derived from [PCIM]Br, [CIM]Br, [PBIM]Br, and [PCPy]Br, respectively.

Table 1. Calculated N_2 adsorption parameters at 77 K for HMC@NC-900 derived from different carbon sources.

Carbon sources	S_{BET} (m ² /g) ^a	V_{SP} (cm ³ /g) ^b	V_{micro} (cm ³ /g) ^c	S_{micro} (m ² /g) ^d
[PCIM]Br	262	0.106	0.072	157
[CIM]Br	278	0.117	0.110	239
[PBIM]Br	133	0.071	0.037	84
[PCPy]Br	58	0.034	0.019	43

^a Specific surface area calculated using the BET equation. ^b Single point pore volume at relative pressure of 0.98. ^c Micropore volume. ^d Micropore surface area.

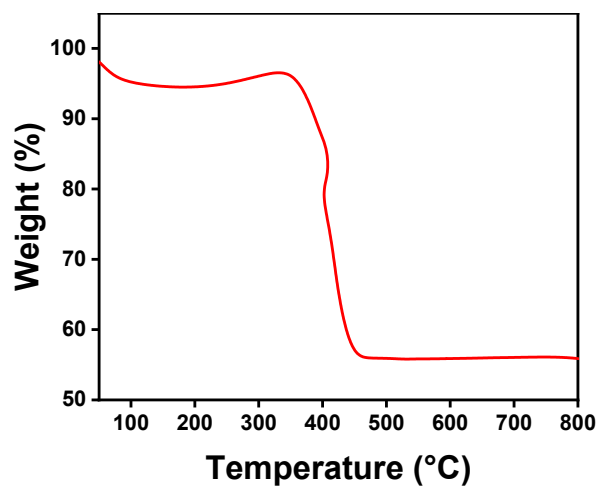


Figure S9. TG analysis for HMC@NC-900.

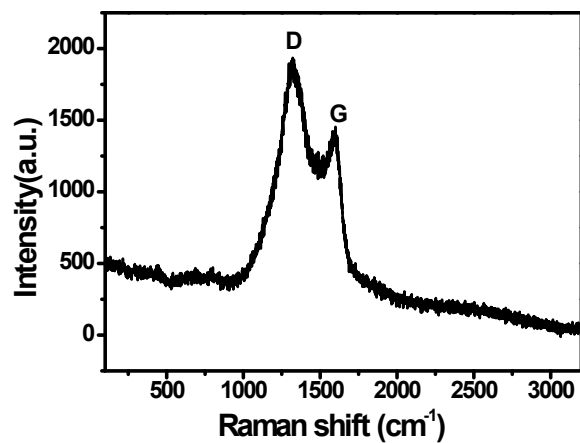


Figure S10. Raman spectrum of HMC@NC-900.

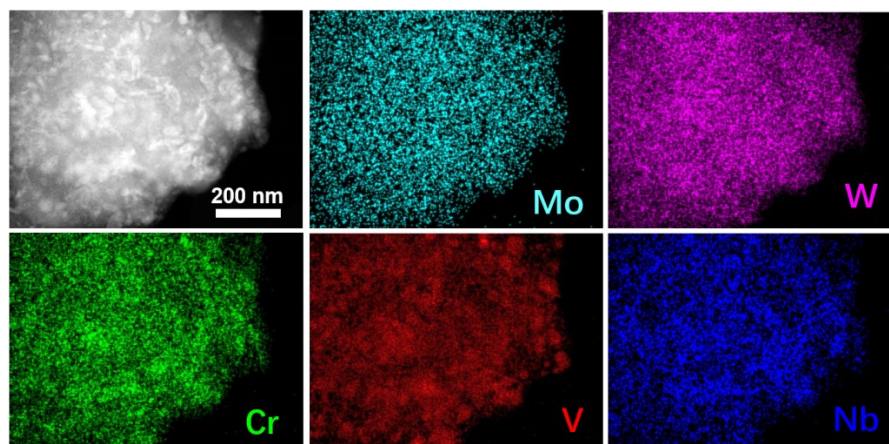


Figure S11. TEM images and EDS maps of Mo, W, Cr, V, and Nb in HMC@NC-900.

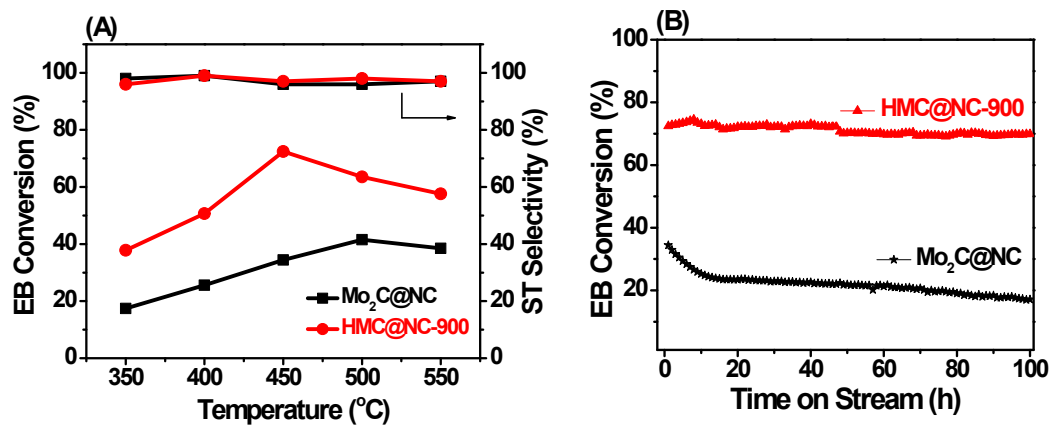


Figure S12. (A) The effect of reaction temperature on the catalytic performance of HMC@NC-900 and Mo₂C@NC in CO₂-DEB; (B) The stability test of HMC@NC-900 and Mo₂C@NC in CO₂-DEB.

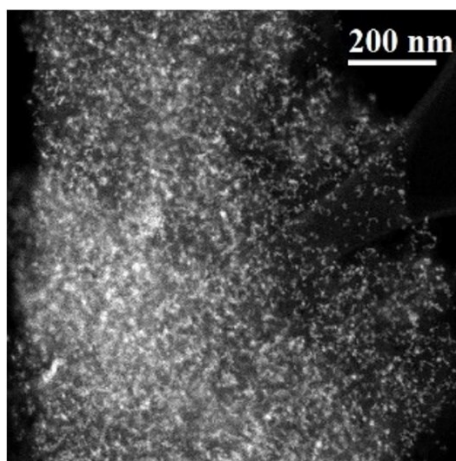


Figure S13. STEM-HAADF image of spent HMC@NC-900 after 100 h.